

# The MaGICC volume: reproducing statistical properties of high redshift galaxies

Rahul Kannan<sup>1\*</sup>†, Greg S. Stinson<sup>1</sup>, Andrea V. Macciò<sup>1</sup>, Chris Brook<sup>2</sup>,  
Simone M. Weinmann<sup>3</sup>, James Wadsley<sup>4</sup>, Hugh M. P. Couchman<sup>4</sup>

<sup>1</sup> *Max-Planck-Institut für Astronomie, Königstuhl 17, 69117 Heidelberg, Germany*

<sup>2</sup> *Departamento de Física Teórica, Universidad Autónoma de Madrid, E-28049 Cantoblanco, Madrid, Spain*

<sup>3</sup> *Leiden Observatory, Leiden University, P.O. Box 9513, 2300 RA Leiden, The Netherlands*

<sup>4</sup> *Department of Physics and Astronomy, McMaster University, Hamilton, Ontario, L8S 4M1, Canada*

6 August 2021

## ABSTRACT

We present a cosmological hydrodynamical simulation of a representative volume of the Universe, as part of the Making Galaxies in a Cosmological Context (MaGICC) project. MaGICC uses a thermal implementation for supernova and early stellar feedback. This work tests the feedback model at lower resolution across a range of galaxy masses, morphologies and merger histories. The simulated sample compares well with observations of high redshift galaxies ( $z \geq 2$ ) including the stellar mass–halo mass ( $M_\star - M_h$ ) relation, the Galaxy Stellar Mass Function (GSMF) at low masses ( $M_\star < 5 \times 10^{10} M_\odot$ ) and the number density evolution of low mass galaxies. The poor match of  $M_\star - M_h$  and the GSMF at high masses ( $M_\star \geq 5 \times 10^{10} M_\odot$ ) indicates supernova feedback is insufficient to limit star formation in these haloes. At  $z = 0$ , our model produces too many stars in massive galaxies and slightly underpredicts the stellar mass around  $L^\star$  mass galaxy. Altogether our results suggest that early stellar feedback, in conjunction with supernovae feedback, plays a major role in regulating the properties of low mass galaxies at high redshift.

**Key words:** galaxies: formation – galaxies: evolution, interactions, structure – methods: numerical – methods: N-body simulations

## 1 INTRODUCTION

Gravitational assembly of structure in a Lambda Cold Dark Matter ( $\Lambda$ CDM) Universe is well understood and mostly consistent with observations. However, the evolution of galaxies inside dark matter haloes presents many challenges for modellers. The baryonic physics in haloes is complicated, involving various processes such as gas cooling, star formation, radiative transfer, stellar and active galactic nucleus (AGN) feedback. These processes are highly non-linear and modelling them accurately is the major challenge for galaxy formation theory.

Fortunately, there are now large catalogues of galactic data available from the local universe to as far back as  $z = 4$ . They make it possible to compare galaxy formation models with observations, throughout their evolution.

These catalogues include observations that present full spectral energy distributions of the galaxies from 1.4 GHz radio continuum observations with the *VLA* (Karim et al. 2011), to infrared imaging with *Hubble/WFC3*, *Spitzer/MIPS* and *VLT/HAWK-I* (Kajisawa et al. 2010; Santini et al. 2012). These observations give a complete picture of star formation even when it is dust obscured.

From these observations, one can construct a cosmic star formation history to compare with models (Lilly et al. 1996; Madau et al. 1996; Hopkins 2004; Wilkins et al. 2008; Bouwens et al. 2012). The shape of the cosmic star formation history has a steep rise from  $z = 0$  to  $z = 1$  before flattening off and then steadily decreasing from  $z = 2$  to higher redshift.

It is also possible to compare the star formation rate (SFR) of individual galaxies with their stellar mass ( $M_\star$ ) determined from infrared photometry. In observations, SFR and  $M_\star$  show a tight correlation that is sometimes called the star forming main sequence (Brinchmann et al. 2004; Noeske et al. 2007; Wuyts et al. 2011). The slope of the relationship does not evolve significantly with redshift, but the

\* Member of the International Max Planck Research School for Astronomy and Cosmic Physics at the University of Heidelberg (IMPRS-HD) and the Heidelberg Graduate School of Fundamental Physics (HGSFP)

† kannan@mpia.de

normalization increases at higher redshifts (Whitaker et al. 2011; Kajisawa et al. 2010).

Dividing the SFR by  $M_*$  gives the specific star formation rate (sSFR), which provides a test of the star formation efficiency compared to prior star formation. Similar to the rise of the star forming main sequence, the sSFR rises with redshift (Karim et al. 2011; Kajisawa et al. 2010). Above  $z = 2$ , some observations show that the evolution of the sSFR flattens, though Stark et al. (2013) found that when corrected for nebular line emission, the sSFR continues increasing up to  $z = 7$ .

The primary constraint used for many models is the number density of galaxies as a function of their stellar mass, the galaxy stellar mass function (hereafter, GSMF). The GSMF is a Schechter type function characterized by a power law at low masses and an exponential cutoff. At  $z = 0$ , the exponential cutoff is at  $M_* \sim 5 \times 10^{10} M_\odot$  (Li & White 2009). The GSMF evolves as a function of redshift: Santini et al. (2012) find that the low mass slope increases with redshift while Peng et al. (2010) finds that the slope remains constant, but the normalization increases.

Three types of models are commonly used to understand how stars populate galaxies:

- Statistical models: compare statistics of simulations with observations
- Semi-analytic models: populate dark matter haloes with stars based on halo mass, merger history, and single zone physics
- Cosmological simulations: Model a volume of the Universe with hydrodynamics

## 1.1 Statistical Models

The statistical models are based on comparing the GSMF with the dark matter halo mass function and lead to an understanding of how efficiently stars form as a function of dark matter halo mass. A set of cosmological parameters makes explicit predictions about the mass function (Press & Schechter 1974; Sheth et al. 2001; Reed et al. 2005) of dark matter haloes and how those haloes are distributed throughout the Universe. The observed GSMF has a different shape than the dark matter halo mass function found in simulations. The GSMF low mass slope ( $\alpha$ ) is shallower than the low mass dark matter mass function slope. The  $M_* \sim 5 \times 10^{10} M_\odot$  cutoff is at a lower mass than the dark matter mass function exponential cutoff.

Halo Occupation Models make the reasonable assumption that the distribution of galaxies in the Universe is similar to the distribution of dark matter haloes, modulo some bias (Peacock & Smith 2000). Halo Occupation Models attempt to match the correlation function statistics of galaxies and dark matter haloes to determine the stellar mass of galaxies that are most likely to be present in a particular dark matter halo. Using Halo Occupation Modelling, one can construct a Conditional Luminosity Function that can be compared with the real luminosity function (Yang et al. 2003; van den Bosch et al. 2007).

Conroy et al. (2006) realized that if one used satellite masses at their time of accretion, then the clustering statistics of mass-ordered dark matter halo samples matches galaxies. This realization led to the abundance matching

technique in which galaxies are placed in dark matter haloes with the same stellar mass ranking as that of the dark matter halo mass rank (Conroy & Wechsler 2009; Moster et al. 2010; Guo et al. 2010; Behroozi et al. 2010). Such a match leads to the *stellar mass-halo mass* ( $M_* - M_h$ ) relationship, the key constraint for our model. The  $M_* - M_h$  relation consists of two power laws with a steep slope at low masses and shallow slope at high masses. Stars form most efficiently at the break mass. The star formation efficiency drops quickly to both higher and lower masses. The characteristic mass of the break in the power law is  $M_{halo} \sim 10^{12} M_\odot$  at  $z = 0$  (Moster et al. 2013).

The availability of luminosity functions at high redshifts means that we can trace the evolution of the  $M_* - M_h$  relation. Abundance matching indicates that the  $M_* - M_h$  relation evolves surprisingly little (Behroozi et al. 2013a). The star formation efficiency evolves most significantly to higher halo masses at higher redshift from  $M_h \sim 10^{12} M_\odot$  at  $z = 0$  to  $M_h \sim 10^{12.5} M_\odot$  at  $z = 3$  (Moster et al. 2013; Behroozi et al. 2013b).

The key finding of the abundance matching models is that the star formation peaks earliest in the highest mass galaxies whereas, in the lowest mass galaxies, the SFR increases monotonically with time. This is a reflection of galaxy downsizing (Fontanot et al. 2009). This represents a delay of star formation in low mass haloes and is the most important feature that must be reproduced in models in order to get the evolution of low mass galaxies right.

## 1.2 Semi-Analytic Models

Semi-Analytic Models (SAMs) try to match the GSMF at  $z = 0$  using physical prescriptions based on the mass and merger history of dark matter haloes taken from simulations (Kauffmann et al. 1993). SAMs show that supernovae can limit star formation in low mass galaxies (White & Rees 1978; White & Frenk 1991; Somerville & Primack 1999; Benson et al. 2003) and that active galactic nuclei (AGN) can limit star formation in high mass galaxies (e.g. De Lucia et al. 2006; Bower et al. 2006).

While SAMs do well matching the evolution of the high mass luminosity function, they do not match the evolution of low mass galaxies at high redshift (Guo et al. 2011). Current SAMs include strong stellar feedback to reproduce the GSMF at  $z = 0$  (e.g. Guo et al. 2011; Bower et al. 2012), but the low and intermediate mass galaxies build their stellar mass at early times ( $z > 2$ ) following the assembly of the dark matter mass, because the feedback mechanism in these SAMs do not delay star formation in low mass haloes. That means that there is little evolution in the SAM luminosity functions after  $z = 2$ , in contrast with observations (e.g. Fontanot et al. 2009; Marchesini et al. 2009; Guo et al. 2011). The early star formation means the SAM galaxies have low specific star formation rates at  $z < 2$  (e.g. Daddi et al. 2007; Damen et al. 2009) and high values at  $z > 3$  (e.g. Bouché et al. 2010; Dutton et al. 2010; Weinmann et al. 2011) although this picture might change at high redshifts due to refinement in the observational estimates of sSFR (Stark et al. 2013). This discrepancy has been looked at in detail by Weinmann et al. (2012), who use the number density evolution of low mass ( $9.27 < \log(M_*/M_\odot) < 9.77$ ) galaxies as a diagnostic to find that

the observed evolution of the number density is not reproduced in any SAMs or simulations. They argue that the simple supernova feedback mechanism used in these models that gets the present day GSMF correct does not decouple star formation from the parent DM halo growth.

### 1.3 Simulations

Hydrodynamical simulations differ from SAMs in that they include self-consistent interaction of dark matter and baryon evolution. Although the efficiency of computational calculations has increased, it is still not possible to resolve many important physical processes, so they must be modelled at the ‘sub-grid’ level. These processes include gas cooling, star formation and stellar feedback.

Since relatively little is known about star formation and feedback, the models include free parameters, which are constrained by observations. Star formation model parameters are constrained using local observations of the Kennicutt-Schmidt gas density–star formation density relation (Springel & Hernquist 2003; Stinson et al. 2006; Schaye & Dalla Vecchia 2008). The energy feedback from stars is modelled either by adding velocity to gas, called *kinetic feedback*, or adding thermal energy as *thermal feedback*. These models have been constrained based on observations (Springel & Hernquist 2003; Oppenheimer & Davé 2006; Dalla Vecchia & Schaye 2008; Crain et al. 2009; McCarthy et al. 2012). The model used in this paper instead constrains stellar feedback to match the evolution of  $M_\star - M_h$  relation.

There has been a lot of research on the optimal velocity for winds driven using kinetic feedback. The original models used a fixed wind velocity (Springel & Hernquist 2003; Crain et al. 2009; McCarthy et al. 2012), however, they had difficulties reproducing the GSMF at  $z = 0$ . Observations of metal absorption lines in outflows show that wind velocities are not constant, but are correlated with star formation rate,  $v_w \approx SFR^{0.35}$ , at  $z = 0$  (Martin 2005) and  $v_w \approx SFR^{0.3}$  at  $z \approx 1.4$  (Weiner et al. 2009). These observations motivated using momentum conserving wind models in which mass loading depends on the mass of the host galaxy such that  $\dot{M}_{wind}/\dot{M}_\star \propto V_{circ}^{-1}$  (Oppenheimer & Davé 2006; Oppenheimer & Davé 2008; Davé et al. 2011a,b). Momentum conserving winds successfully reproduce the GSMF and many other observed galaxy properties at  $z = 0$  (Oppenheimer et al. 2010; Davé et al. 2011a,b; Puchwein & Springel 2013), but has similar shortcomings with the low mass end of the luminosity function as the SAMs at high redshift. Weinmann et al. (2012) conclude that the current models of stellar feedback (in both SAMs and simulations) are unlikely to decouple the galaxy and DM halo growth due to its fundamental dependence on host halo mass and accretion history. An alternative to the momentum driven wind model is the energy conserving approximation for driving outflows from galaxies in which the mass loading factor scales as  $\dot{M}_{wind}/\dot{M}_\star \propto V_{circ}^{-2}$ . Puchwein & Springel (2013) find that using this approximation of a stronger scaling of mass loading with galaxy size results in a shallower slope of the GSMF at  $z = 0$ . The energy driven wind model also suppresses star formation at high redshift, reducing the cosmic star formation rate density to observed levels and

shifting its peak to  $z \sim 2.5$ . This model is also successful in reproducing the GSMF at  $z = 1$  and  $z = 2$  reasonably well.

In thermal stellar feedback, stars heat the surrounding gas particles adiabatically, which creates pressure that can push gas out of galaxies (Gerritsen & Icke 1997; Thacker & Couchman 2000; Kawata & Gibson 2003; Stinson et al. 2006). SNe energy can only efficiently drive outflows if the Sedov-Taylor phase of gas expansion is resolved. Such resolution is infeasible even with modern computer hardware, so two techniques have been employed to model this sub-grid physics. Stinson et al. (2006) delay cooling within the blast region that a supernova would create. Dalla Vecchia & Schaye (2012) integrate all the supernova energy that a stellar population creates and put it in a single gas particle. This raises the temperature to lengthen the cooling time enough so that the hot gas particle has a dynamical effect.

Simulations using thermal feedback have so far focused on disk structure using high resolution zoom in simulations (Governato et al. 2010; Brook et al. 2011; Sawala et al. 2011; Guedes et al. 2011; Agertz et al. 2011). Some recent simulations of a handful of galaxies have indicated that adiabatic feedback produces galaxies that follow  $M_\star - M_h$  below  $M_{halo} < 10^{12} M_\odot$  (Brook et al. 2012; Munshi et al. 2013).

In most models of stellar feedback, only feedback from supernovae is considered, but Murray et al. (2010) recognized the amount stars can disrupt molecular clouds before any stars explode as supernovae. Hopkins et al. (2011) and Agertz et al. (2013) implemented early stellar feedback schemes that rely on IR radiation pressure and tested them on isolated galaxy simulations. Lopez et al. (2011) and Pellegrini et al. (2011) found that when they mapped the pressure in different phases of the gas in the 30 Doradus region of the LMC, UV photoheating provides more pressure than IR radiation pressure.

In Stinson et al. (2013), we assume that photo-heating from massive stars is thermalised by the time it reaches the spatial scales resolved in cosmological simulations. So, we inject thermal energy equal to the fraction of the bolometric luminosity emitted in the UV in the time between the formation of the star and the first supernova explosion. This early stellar feedback limits star formation to the amount prescribed by the  $M_\star - M_h$  relationship and delays star formation in an  $L_\star$  galaxy, so that the galaxy follows the evolution of the  $M_\star - M_h$  relationship. This is a major improvement over previous galaxy formation models, as the delayed star formation means that star formation is decoupled from DM halo mass growth. Some side-effects of using early stellar feedback include transforming DM cusps to cores in galaxies up to  $L_\star$  masses (Macciò et al. 2012) and populating the circum-galactic medium with hot metal enriched gas, matching OVI observations (Stinson et al. 2013).

In this paper, we explore how the early stellar feedback model, described in Stinson et al. (2013), affects the global properties of galaxies on a large scale. To study this we simulate a large volume of the Universe, 114 Mpc on a side, as part of the Making Galaxies in a Cosmological Context (MaGICC) project. This simulation tests the effectiveness of our model at low resolution across a wide range of galaxy masses, environments and merger histories. We compare the properties of the galaxies in our simulations with observed statistical properties of high redshift galaxies like the GSMF,

stellar to halo mass relationship, star formation rate, and the number density evolution of low mass galaxies through cosmic time. In Section 2 we briefly outline the star formation and stellar feedback mechanisms used in our simulations, in Section 3 we present our results at  $z \geq 2$  and compare them to the current observational estimates. In Section 5 we summarize our results and discuss future challenges.

## 2 SIMULATION METHOD

We simulate a cosmological volume, 114 Mpc on a side, from  $z = 99$  to  $z = 2$ . It is created using WMAP7 initial conditions with  $(h, \Omega_M, \Omega_\Lambda, \Omega_b, \sigma_8) = (0.702, 0.2748, 0.7252, 0.0458, 0.816)$  (Larson et al. 2011; Komatsu et al. 2011). The simulation includes  $512^3$  dark matter and  $512^3$  gas particles. The dark matter particle has mass of  $3.4 \times 10^8 M_\odot$  and a softening length of  $\sim 3.7$  kpc. The initial gas particle mass is  $6.9 \times 10^7 M_\odot$  and the initial star particle mass is  $1.3 \times 10^7 M_\odot$ . Gas and star particles have a softening length of  $\sim 2.17$  kpc. §4 describes lower resolution simulations that were used to test the resolution dependence of our model.

All the simulations use the smoothed particle hydrodynamics (SPH) code GASOLINE (Wadsley et al. 2004). The smoothing length is calculated using 32 nearest neighbours. Details of the physics used in the MaGICC project are detailed in Stinson et al. (2013). Briefly, stars are formed from gas cooler than  $T = 10^4$  K, and denser than  $8.7 \text{ cm}^{-3}$  according to the Kennicutt Schmidt Law as described in Stinson et al. (2013) with the star formation efficiency parameter  $c_* = 0.1$ . The cooling used in this paper is described in detail in Shen et al. (2010). It was calculated using CLOUDY (version 07.02; Ferland et al. 1998) including photoionisation and heating from the Haardt & Madau (unpublished) ultraviolet (UV) background, Compton cooling, and hydrogen, helium and metal cooling from 10 to  $10^9$  K.

The star particles are massive enough to represent an entire stellar population consisting of stars with masses given by the Chabrier (2003) initial mass function. 20% of these have masses greater than  $8 M_\odot$  and explode as Type II supernovae from 4 until 35 Myr after the stellar population forms according to the Padova stellar lifetimes (Alongi et al. 1993; Bressan et al. 1993). Each supernova ejects  $E_{SN} = 10^{51}$  ergs of purely thermal energy into the surrounding gas ( $\sim 1$  kpc at the resolution of our simulations). The supernova energy would be radiated away before it had any dynamical impact because of the high density of the star forming gas. Thus, the supernova feedback relies on delaying the cooling based on the sub-grid approximation of a blast wave as described in Stinson et al. (2006).

The supernovae feedback does not start until 3.5 Myr after the first massive star forms. However, nearby molecular clouds show evidence of being blown apart *before* any SNII exploded (Murray et al. 2011). Lopez et al. (2011) and Pellegrini et al. (2011) found that UV photoheating is the dominant feedback mechanism in early phases of star formation by mapping out the pressure in different phases of the gas. In simulations in the MaGICC project, like those here, 10% the UV luminosity of the stars is injected into the surrounding gas over this 3.5 Myr period without disabling the cooling, at the rate of  $4.45 \times 10^{48} \text{ erg/Myr}/M_\odot$ . Stinson et al. (2013) showed that this energy limits star for-

mation to the amount prescribed by the  $M_* - M_h$  relationship at all redshifts. The current work is our attempt explore how this star formation and feedback prescription works at lower resolutions over a wide range of galaxy masses.

### 2.1 Halo identification

For each snapshot, we find all the virialised haloes within the high resolution region using a Spherical Overdensity (SO) algorithm. Candidate groups with a minimum of  $N_f = 100$  particles are selected using a FoF algorithm with linking length  $\phi = 0.2d \approx 22$  kpc ( $d$  is the mean inter-particle separation). We then: (i) find the point  $C$  where the gravitational potential is a minimum; (ii) determine the radius  $\bar{r}$  of a sphere centred on  $C$ , where the density contrast is  $\Delta_{\text{vir}}$ , with respect to the critical density of the Universe. Using all particles in the corresponding sphere of radius  $\bar{r}$ , we iterate the above procedure until we converge onto a stable particle set. This stable particle set is then defined as a ‘halo’. A galaxy is all stars within the particle set defined as a ‘halo’. This does not affect the definition of stellar mass in low mass galaxies, the focus of this paper, because their substructures contain very little amount of stars. We use a constant virial density contrast  $\Delta_{\text{vir}} = 200$ , in order to be consistent with Moster et al. (2013). We include in the halo catalogue all the haloes with more than 100 particles (see Macciò et al. 2007, 2008 for further details on our halo finding procedure).

## 3 RESULTS

We compare the simulated galaxy population in a  $114^3 \text{ Mpc}^3$  volume with a set of basic properties derived from the most recent observational estimates. These include the galaxy stellar mass function (GSMF), stellar mass–halo mass ( $M_* - M_h$ ) relationship, cosmic star formation history (SFH), star forming main sequence, and specific star formation rates (sSFRs). Individual galaxies have been shown to match observations well (Brook et al. 2012; Stinson et al. 2013), so the volume provides an opportunity to test the accuracy and effectiveness of this feedback model at low resolution and high redshift. All the observational estimates of stellar masses and SFRs, that our results have been matched to, have been corrected to a Chabrier (2003) IMF. The results presented in this paper have all been presented in comoving units where ever applicable.

### 3.1 Stellar - halo mass ( $M_* - M_h$ ) relation

Figure 1 shows the  $M_* - M_h$  relation for all the galaxies in the simulated volume (black points) that contain a minimum of 20 star particles, or a stellar mass of  $\sim 3 \times 10^8 M_\odot$ . The galaxies trace (red solid line) the slope of the  $M_* - M_h$  (green line) up to  $M_{\text{halo}} = 10^{12} M_\odot$  at all redshifts where it has been examined. The scatter of the simulated galaxies, quantified by the 10 and 90 percentile limits of the distribution (red dotted lines), also matches the variation in the relation as obtained by Moster et al. (2013) (grey shaded area). The agreement points to the fact that the stellar feedback effectively regulates star formation to produce the right amount of stellar mass in a given halo mass at all times.



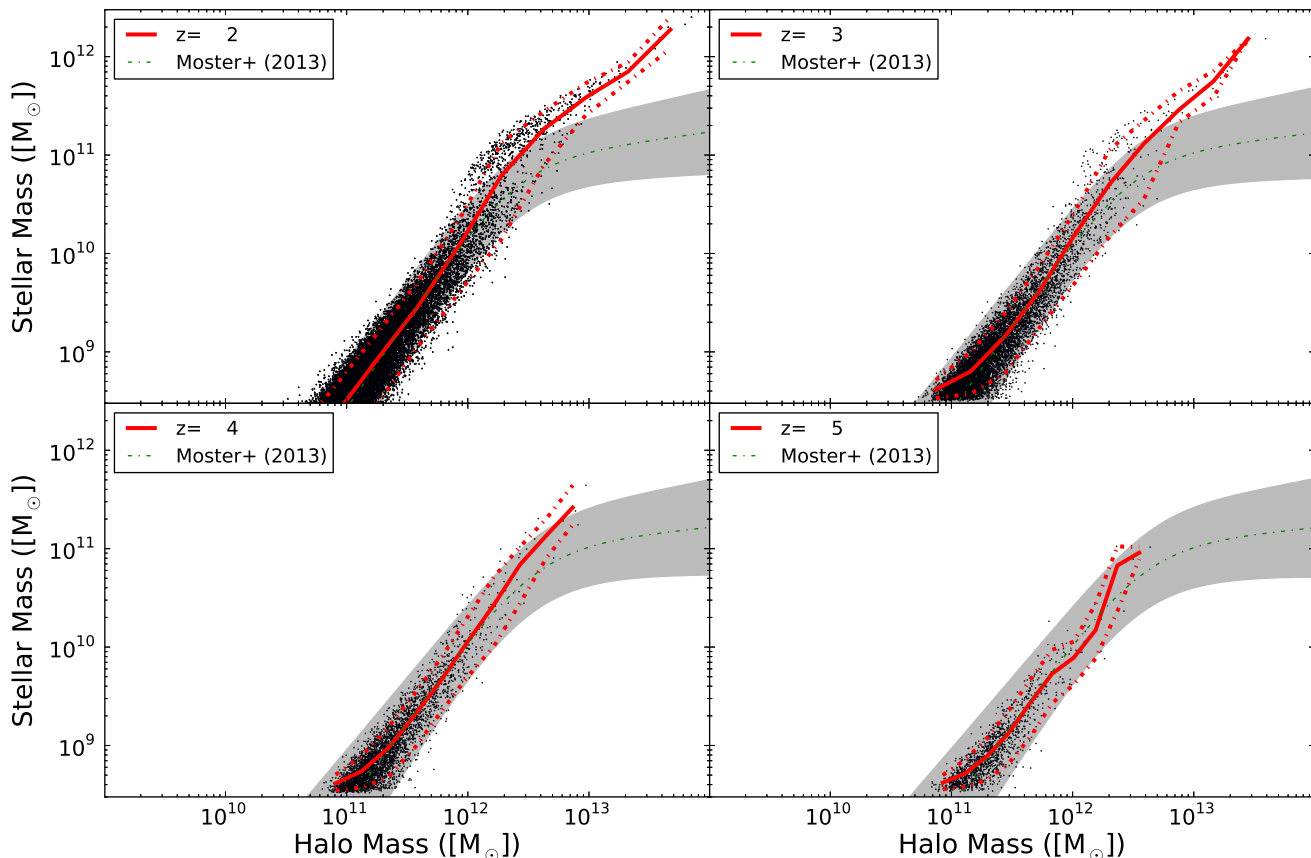


**Figure 1.**  $M_* - M_h$  relation at different redshifts. The black points are simulated galaxies, with the red solid line tracing the mean of the distribution and the red dotted lines indicate the 10 and 90 percentile limits of the distribution. The green dotted line is the Moster et al. (2013) relation derived from abundance matching techniques and the grey shaded area is the scatter derived for the relation. Our simulated galaxies match the relation below  $M_{halo} < 10^{12} M_\odot$ , but star formation is too efficient in high mass haloes.

Above a halo mass of  $10^{12} M_\odot$ , abundance matching (green dotted line) shows a decrease in star formation efficiency. This is not reproduced in the simulation. The star formation efficiency actually increases at  $M_{halo} \sim 4 \times 10^{12} M_\odot$ , before decreasing slightly as represented by the slightly shallower slope of the simulation points. The reduced SFE is due to the reduced gas accretion because of the high virial gas temperature of the halo. However, this slight decrease in SFE does not reduce the star formation in these high mass haloes to the extent observed. The implemented stellar feedback model is insufficient in these high mass haloes. Some other quenching mechanism is required such as feedback from a central super-massive black hole (AGN feedback, e.g. Fanidakis et al. 2011; Springel et al. 2005).

### 3.2 The galaxy stellar mass function (GSMF)

The GSMF measures the number of galaxies of a certain stellar mass in a given volume of the Universe. The era of deep, high redshift surveys has provided detailed GSMFs out to  $z = 3$ . We compare our simulation results to Santini et al.

(2012), who use deep *WFC3* near-IR data complemented by deep *Hawk-I*  $K_S$  band data to derive accurate stellar masses in a  $\sim 33$  arcmin<sup>2</sup> area located in the GOODS-South field, to study the low-mass end of the GSMF. The observed GSMFs are presented for various redshift ranges. To compare with them, we use the simulated GSMF from the middle of the observed redshift range. Figure 2 shows that the simulated galaxies from the fiducial run (blue line) trace the intermediate mass ( $10^{9.5} < M_*/M_\odot < 10^{11}$ ) slope of the observed GSMF (red points) very well. There is a slight discrepancy at  $M_* < 10^{9.5} M_\odot$  at  $z = 2.15$ . This discrepancy might arise due to the difficulty in determining the properties of low mass galaxies at such large distances or due to cosmic variance, as their data set has a small sky coverage. The feedback model makes the slope of the GSMF as shallow as the observed value, which is non-trivial and is a major improvement over previous attempts to match the GSMF at high redshift (e.g. Guo et al. 2011). A small discrepancy remains, as the simulated number density of high mass galaxies continues to decrease at the same rate, whereas the observations show an exponential cutoff. This again indicates that stellar feedback is insufficient to limit

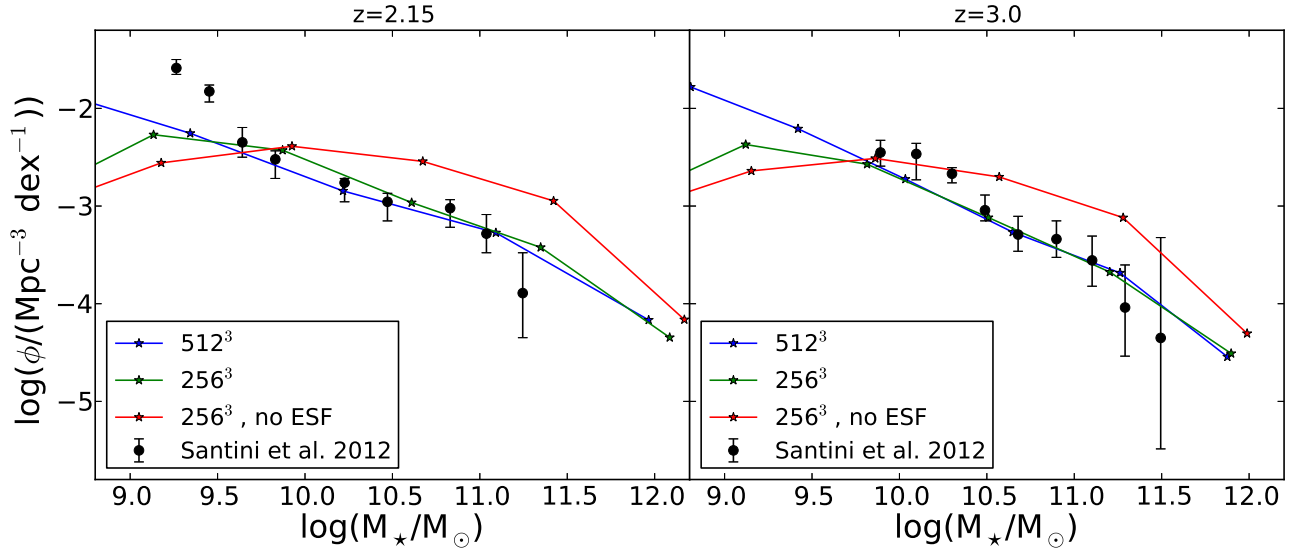


**Figure 2.** Galaxy stellar mass function at  $z \sim 2$  and  $z = 3$  compared to observational data taken from Santini et al. (2012) for three different simulations. The fiducial simulation with  $512^3$  particles is shown in blue, the corresponding low resolution run ( $256^3$ ) is shown in green, while the low resolution simulation without ESF is coloured red.

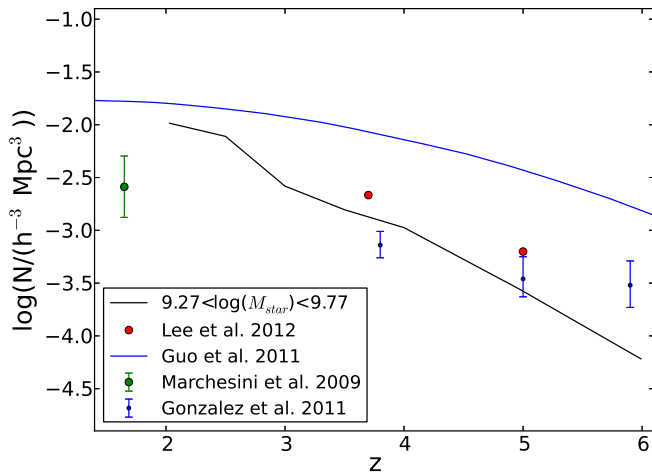


**Figure 3.** Number density of low mass galaxies as a function of redshift (black line) compared to various observational estimates (points) and a semi analytic model (blue line) as described in Guo et al. (2011). Our simulation results have a steeper slope and are a better fit to the observational data.

star formation in these high mass haloes. The green and red curves are control test runs, which will be discussed in §4.

### 3.3 Number density evolution of low mass galaxies

Weinmann et al. (2012) used the number density evolution of low mass ( $9.27 < \log(M_*/M_\odot) < 9.77$ ) galaxies to show that semi-analytic models or cosmological hydrodynamic simulations do not correctly model low mass galaxies. They argue that the simple supernova feedback mech-

anism changes the stellar mass at  $z = 0$ , but renormalizes the star formation history and thus does not decouple star formation from DM accretion. Stinson et al. (2013) showed for a single high resolution  $L^*$  simulation that early stellar feedback can break the coupling of star formation to dark matter accretion. Figure 3 shows the number density evolution of low mass galaxies at high redshifts in our simulation volume compared to observations taken from Figure 1 of Weinmann et al. (2012), as well with the SAM described in Guo et al. (2011). The simulation matches the observational results much better and lies well below the values obtained by the SAM. The difference between the observations of González et al. 2010 (blue points) and Lee et al. 2012 (red points) is larger than the González et al. 2010 error bars. The simulated curve falls in the middle of these observations in contrast with the SAM that lies an order of magnitude above the observations. We note that the slope obtained from our model is still slightly steeper than observed, indicating that the simulation is building low mass galaxies faster than observed.

### 3.4 Star formation History

We can also compare our simulation with the total number of stars formed in the Universe as a function of time. Figure 4 shows how the cosmic star formation rate evolves as a function of redshift (‘Lilly-Madau plot’) in our simulated volume. The observed points used for comparison are taken from Moster et al. (2013) and include star formation estimates derived from rest frame UV (Salim et al. 2007; van der Burg et al. 2010; Robotham & Driver 2011; Bouwens et al. 2011; Cucciati et al. 2012),  $H\alpha$  (Ly et al. 2011), combined UV and IR (Zheng et al. 2007; Kajisawa et al. 2010), FIR (Rujopakarn et al. 2010) and radio observations (Smolčić et al. 2009; Dunne et al. 2009; Karim et al. 2011).

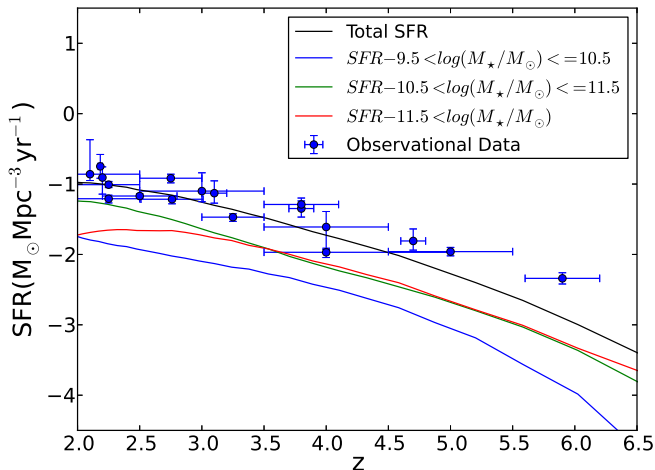


**Figure 4.** The evolution of the star formation rate density. The blue points are a compilation of star formation rate density estimates taken from Moster et al. (2013). The black solid line is our result for all galaxies in our volume. The coloured curves show the star formation histories of galaxies in a certain mass range. The mass of galaxies quoted is calculated at  $z = 2$ . The blue line is the SFR density for low mass galaxies ( $9.5 < \log(M_*/M_\odot) < 10.5$ ), the green for intermediate ( $10.5 < \log(M_*/M_\odot) < 11.5$ ) mass galaxies and the red line for high mass ( $\log(M_*/M_\odot) > 11.5$ ) galaxies. There is a clear trend of decreasing star formation at  $z \leq 3.5$  in the highest mass galaxies.

The total SFR density (black line) passes through the observations from  $z = 2 - 5$ .

The total SFH can be divided into separate lines based on the stellar mass of the halo at  $z = 2$  in which the stars are formed. The lowest mass galaxies ( $9.5 < \log(M_*/M_\odot) < 10.5$ ) contribute little to the overall SFR density, while the intermediate ( $10.5 < \log(M_*/M_\odot) < 11.5$ ) and high mass ( $\log(M_*/M_\odot) > 11.5$ ) contribute equally up to  $z = 3$ . Below this redshift, the SFR flattens out in the highest mass galaxies. This flattening is not sufficient to explain the quenching of high mass galaxies as shown by the failure of the simulated  $M_* - M_h$  and GSMF relations at the high mass end. We note that our match of the star formation history is not greatly affected by the excess star formation in galaxies with ( $\log(M_*/M_\odot) > 11.5$ ) because even though the galaxies in that mass range form too many stars at  $z \leq 3.5$ , they are not the dominant population of galaxies at those redshifts.

### 3.5 Star forming main sequence

Observations show that star-forming galaxies have a tight correlation between their SFR and  $M_*$  (e.g., Elbaz et al. 2007; Pannella et al. 2009; Wuyts et al. 2011; Whitaker et al. 2012). This correlation has been called the “star forming main sequence.”

We compare the SFRs of our simulated galaxies with observational estimates by Kajisawa et al. (2010) and Whitaker et al. (2012). Kajisawa et al. (2010) studied SFR as a function of  $M_*$  for galaxies at  $0.5 < z < 3.5$  in the GOODS-North field, using the K-selected sample from

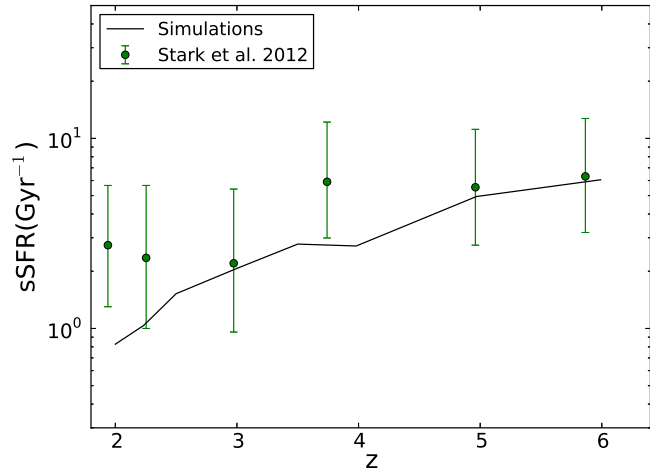


**Figure 6.** The evolution of the specific star formation rate for sample galaxies which have stellar masses within a narrow range around  $\sim 5 \times 10^9 M_\odot$  (blackline). We compare the simulations with the observational estimates of Stark et al. (2013). The evolution of sSFR matches well at  $z \leq 3$ , but is below the observed value at lower redshifts.

*Subaru-MOIRCS*. They determined SFRs from rest-frame, dust-corrected UV luminosity and the *Spitzer*-MIPS  $24 \mu\text{m}$  flux. The depth of their data allowed them to constrain the slope of the SFR- $M_*$  relation down to  $M_* = 10^{9.5} M_\odot$  at  $z \sim 3$ . The median SFR as a function of stellar mass (green curve) from their sample of galaxies is plotted in top panels Fig. 5 at  $z = 2$  & 3. The slope of their relation is close to unity for low mass galaxies at these high redshifts. Our simulated galaxies match these observations well at  $z = 3$ , but have nearly two times less star formation at  $z = 2$ . This discrepancy at  $z = 2$  presents a challenge for all hydrodynamic simulations and SAMs (Weinmann et al. 2011). Davé (2008) suggested that an evolving stellar IMF is required to reduce the discrepancy in this relation out to  $z = 2$ .

Whitaker et al. (2012) measure star formation rates using the NEWFIRM Medium-Band Survey from MIPS  $24 \mu\text{m}$  fluxes. At  $z > 2$  their detection limit is  $\log(M_*/M_\odot) > 10.7$ . For these galaxies, they find a shallower, sub-linear, slope for their star forming main sequence,  $SFR \propto M^{0.44}$ , with a constant scatter of 0.34 dex. Above their detection limit, our simulated galaxies (black points) lie below the observations (red line) as seen in the top left panel of Fig. 5.

Galaxies above a stellar mass of  $10^{11} M_*$  show a slight reduction in star formation rate from the trend at lower masses. This reduction is likely the result of the high temperatures of the gas haloes surrounding these galaxies, which has a long cooling time, so gas accretion onto the disk is slightly reduced. However, observations of such galaxies show a much more dramatic decrease in star formation that is not captured in these simulations.

### 3.6 Specific star formation rate evolution

Another common way to compare star formation rates with galaxy stellar masses is the specific star formation rate

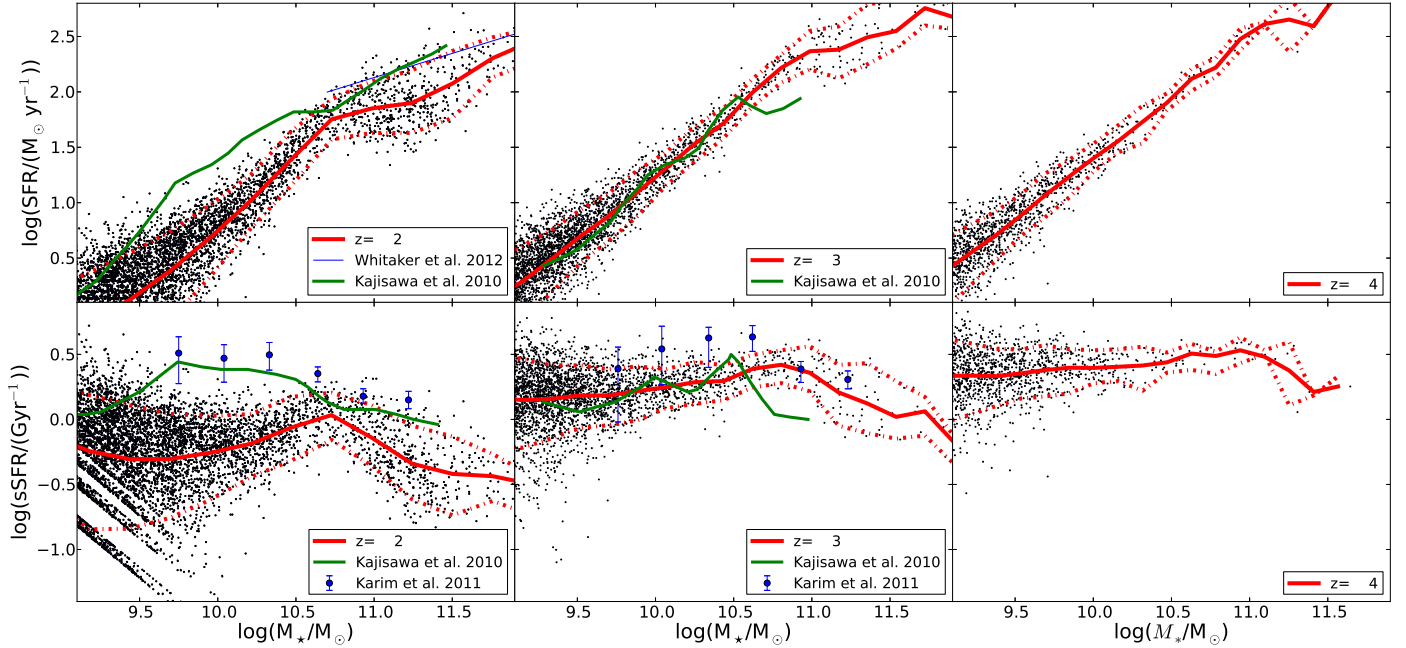


**Figure 5.** Top panels: The star forming main sequence (black points) at different redshifts. The  $z = 2$  result for galaxies with  $\log(M_*/M_\odot) > 10.7$  is matched to the observational results of Whitaker et al. (2012) (Red line). The slope of the main sequence is much steeper at lower masses. This matches well with the observational estimates derived by Kajisawa et al. (2010) at  $z = 2$  & 3 (green curve). Bottom panels: The simulated sSFR (black points) matched to observational results matched from Karim et al. (2011) (Red points) and Kajisawa et al. (2010) (green curve). The simulated sSFR lies below the observed values for low mass galaxies at  $z = 2$  by a factor of  $\sim 2$ , but matches very well at  $z = 3$ .

(sSFR), which gives the amount of star formation in haloes for a unit stellar mass of material. As one would expect from the star forming main sequence, the bottom panels of Fig. 5 show that the simulated galaxies (black points) match the Kajisawa et al. (2010) (green curve) observed sSFRs at  $z = 3$  but have  $\sim 2$  times lower sSFR at  $z = 2$ . We also compare our simulated results with 1.4 GHz radio continuum observations from Karim et al. (2011) of star formation in galaxies in the 2 deg<sup>2</sup> COSMOS field. The simulated galaxies in our volume (black points) are in good agreement above  $\log(M_*/M_\odot) > 10.7$ , but are 2 – 3 times lower below this mass range at both  $z = 2$  & 3.

Karim et al. (2011), like other authors before them (Stark et al. 2009; González et al. 2010), found that sSFR increases for galaxies in a given stellar mass range from  $z = 0$  to  $z \sim 2$ , but then does not evolve much from  $z = 2$  to  $z \sim 7$ . Weinmann et al. (2011) shows that such observations are contradictory with most models in which higher gas accretion rates at higher redshift and lower galaxy stellar masses translate into larger sSFR in galaxies within a fixed stellar mass range.

Stark et al. (2013) re-examined their data and found that their *Spitzer*-IRAC photometry was contaminated by nebular emission. They use the photometric excesses in the contaminated [3.6] filter to estimate the equivalent width distribution of H $\alpha$  emission at  $3.8 < z < 5.0$ . The corrected sSFRs increase from  $z = 4$  to  $z = 7$  by a factor of  $\sim 5$  similar to model predictions. Figure 6 shows the evolution of the sSFR in simulated galaxies (black line) within a narrow stel-

lar mass range around  $\sim 5 \times 10^9 M_\odot$ . The simulation values are consistent with the corrected Stark et al. (2013) values (green points) for  $z > 3$ . However at  $z < 3$  our simulation results are below the observed relation.

Many other authors find also find lower than observed sSFRs in their models (Davé 2008; Weinmann et al. 2012). The higher observed sSFRs again indicates delayed star formation in low mass galaxies. Although our model does a better job of delaying the star formation at early times than most SAMs and hydrodynamic simulations, below  $z = 3$  the simulated haloes may still be forming too few stars. This suggests the importance of some other physical mechanism, not modelled in our simulation, like the dependence of the star formation on gas metallicity (Krumholz et al. 2011; Krumholz & Dekel 2012), that could further delay star formation at earlier times and increase the sSFR of these galaxies at  $z = 2$ .

### 3.7 Results at $z = 0$

Galaxies in the local Universe are the easiest to observe and compare with our model. Unfortunately, it is too computationally demanding to simulate the full cosmological volume to  $z = 0$ . So, we select a  $16 h^{-1}$  Mpc sub-volume from the fiducial simulation at  $z = 2$ . The region was selected to limit the number of high mass haloes present in the region. The lack of massive haloes reduces the computational cost but also reduces the density of the region by  $\sim 10\%$  compared to the mean density for full volume. This kind of volume selec-

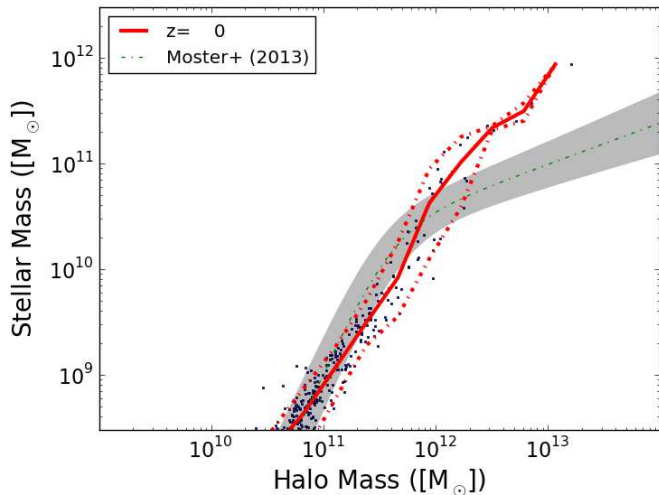


**Figure 7.** The stellar-halo mass relation for galaxies in a  $16 h^{-1}$  Mpc at  $z = 0$ . Galaxies around  $M_{\text{halo}} = 10^{11} M_{\odot}$  have about half the expected stellar mass. Galaxies with  $M_{\text{halo}} > 10^{12} M_{\odot}$  continue to exhibit the overcooling problem like they did at high redshift. The solid red line is the median of the simulation points, while the dotted lines show the 10 and 90 percentile limits for those bins.

tion also impairs our ability to compare the volume weighted properties of galaxies like the GSMF. On the other hand, the individual properties of galaxies like the stellar mass compared to the halo mass of the galaxy ( $M_{\star} - M_h$  relation) and the star formation rate compared to their stellar mass (star formation main sequence) are expected to remain similar irrespective of the surrounding density field. Sheth & Tormen (2004) showed that halo formation weakly depends on the surrounding density field. So, only the  $M_{\star} - M_h$  relation and the star formation main sequence obtained from the selected region are shown at  $z = 0$  in Figs. 7 and 8.

We include gas particles only inside the  $16 h^{-1}$  Mpc sub-volume. Outside this region the particles are re-binned to a lower resolution in order to save computing time. The simulation was then restarted from  $z = 2$  and allowed to continue to  $z = 0$ , with all the other parameters unchanged from the fiducial run. This region contained enough galaxies for us to make a statistical comparison at  $z = 0$  with observations.

Fig. 7 shows the ( $M_{\star} - M_h$ ) relation for the galaxies in the selected cube at  $z = 0$ . The black points are simulated galaxies, the red solid line traces the mean of the distribution and the red dotted lines indicate the 10 and 90 percent confidence intervals of the distribution. The green dotted line is the Moster et al. (2013) relation derived from abundance matching techniques and the grey shaded area is the scatter derived for the relation. The simulation still provides a fair match to the observations at  $M_h \sim 10^{11} M_{\odot}$ , though the galaxies at  $z = 0$  have half the stellar mass of the observed galaxies. The over-cooling problem also remains in higher mass galaxies ( $M_h > 10^{12} M_{\odot}$ ).

As mentioned in §1, previous studies using momentum driven winds SNe feedback recipes (e.g. Oppenheimer et al. 2010, Crain et al. 2009) also tend to overproduce the stellar mass of massive galaxies and slightly under predict the

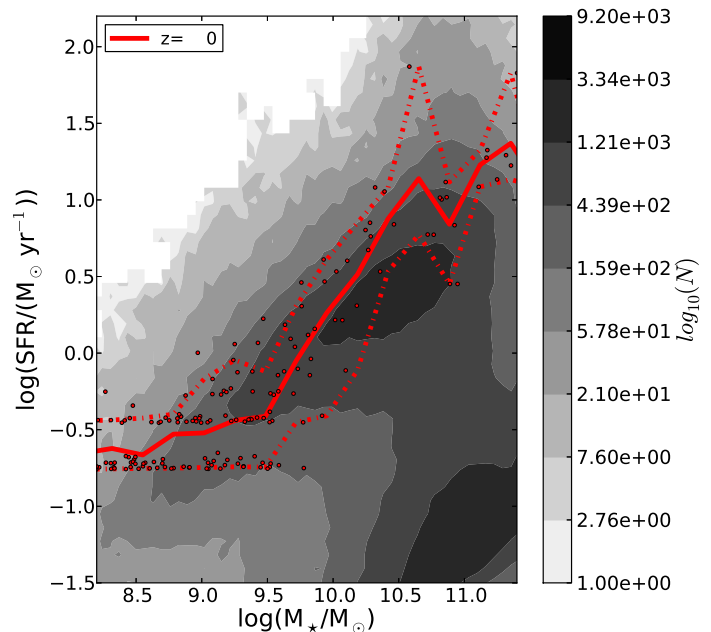


**Figure 8.** The simulated star forming main sequence at  $z = 0$ . Individual galaxies are the red points while the solid red line represents the median of those galaxies. The dot-dashed lines represent the 10 and 90 percentile limits of the galaxy distribution. The simulations are compared with 894k galaxies from SDSS as in Brinchmann et al. (2004) plotted as the grey contours.

stellar mass at the knee of the stellar mass function. Energy driven variable wind models seem to be capable of reproducing the low- $z$  GSMF (for e.g. see Puchwein & Springel 2013). Our model is more successful in reproducing the galaxy stellar mass function at high redshift ( $z > 2$ ) in the low mass galaxy regime, while the previous studies largely overpredict the number of low mass galaxies at these high redshifts (as shown in Fig. 1 of Weinmann et al. 2012) and the differences between observations and our model at  $z = 0$  is pretty small and comparable to previous works.

Observations of the star forming main sequence are also more complete at  $z = 0$ . Fig. 8 shows how the simulated galaxies compare to those observations (grey contours from Brinchmann et al. 2004). The median star formation rates of the simulated galaxies are  $\sim 0.5$  dex higher than the locus of the observed star forming main sequence, but are still within the observed range of star formation rates. This is a change from high redshift where the simulated galaxies had systematically lower star formation rates than observations.

No simulated galaxies populate the quiescent–high stellar mass corner of the plot. Even at  $z = 0$ , the simulation cannot produce red, dead galaxies most likely due to the lack of AGN feedback.

While the simulations have trouble at high masses, this sample of galaxies at  $z = 0$  suggests that the simulations model the static properties of low mass galaxies well throughout the history of the Universe.



#### 4 EFFECT OF RESOLUTION AND EARLY STELLAR FEEDBACK

To test the effect of resolution and early stellar feedback, we simulated the fiducial volume at a lower resolution containing  $256^3$   $2.76 \times 10^9 M_\odot$  dark matter and  $256^3$   $5.5 \times 10^8 M_\odot$  gas particles. Star particles form with masses of  $1.83 \times 10^8 M_\odot$ . The dark matter particles use a softening length of  $\sim 3.7$  kpc, while the gas and star particles use a softening length of  $\sim 2.17$  kpc. All the other simulation parameters are the same as used in the fiducial run. The low resolution simulation was performed with two different feedback models, one with SNe feedback only, and the other adding early stellar feedback to the SNe feedback.

Fig. 2 shows the GSMF’s for these simulations (green and red lines) in addition to the fiducial run (blue curve). The low resolution volume with the same physics as the fiducial run (green curve) matches the fiducial run and observations for  $M_* > 10^{9.5} M_\odot$ . The simulation without early stellar feedback has too many galaxies with  $M_* > 10^{10} M_\odot$ . The decrease in the number of  $M_* > 10^{9.5} M_\odot$  in the low resolution simulations is caused by the resolution limit. These galaxies consist of only a couple star particles, so star formation is not well sampled and the results cannot be trusted. Fig. 2 shows that our model is fairly well converged as well as the need for early stellar feedback to produce realistic galaxies.

#### 5 DISCUSSION AND CONCLUSIONS

We examine the effect of early stellar feedback used in the Making Galaxies in a Cosmological Context (MaGICC) project on a broad sample of galaxies in a cosmological volume of  $114^3$  Mpc<sup>3</sup>. The stellar feedback used is exactly the same as that used for a high resolution  $L_*$  galaxy (Stinson et al. 2013). We compare the simulated galaxies with the observed  $M_* - M_h$  relation, the galaxy stellar mass function, the cosmic star formation history, the star forming main sequence and the specific star formation rate. The simulated galaxies do a good job matching each observation to  $z = 2$ , the time when previous models have most deviated from observations. Our use of early stellar feedback is the key difference between our simulation and ones run previously. The way that it delays star formation in  $M_h < 10^{12} M_\odot$  galaxies allows the simulations to match many observed statistical properties of high redshift galaxies.

At  $z \geq 2$ , the simulated galaxies not only follow the  $M_* - M_h$  for  $M_h < 10^{12} M_\odot$  at all the redshifts examined but also match the scatter in the relation. Correspondingly, the simulated galaxies match the shallow slope at the low mass end of the galaxy stellar mass function. The slope of the GSMF relationship was not a constraint for the simulation, but is a natural by product of the stellar feedback recipe used. It is a major improvement over previous attempts to match the GSMF at high redshift. The early stellar feedback decouples the growth of stellar mass from DM mass by effectively blowing the gas away from the disc either into the circum-galactic medium or entirely out of the halo. This helps regulate the number density of low mass galaxies to the observed values by delaying star formation in these haloes.

The simulated star formation history of the Universe

also matches a variety of different observations. The model predicts that the lowest mass galaxies ( $9.5 < \log(M_*/M_\odot) < 10.5$ ) contribute little to the overall SFR density, while the intermediate ( $10.5 < \log(M_*/M_\odot) < 11.5$ ) and high mass ( $\log(M_*/M_\odot) > 11.5$ ) galaxies contribute equally up to  $z = 3$ . After  $z = 3$ , the star formation slows in the highest mass galaxies.

At  $M_h > 10^{12} M_\odot$ , too many stars form, which is shown by the presence of galaxies above the abundance matching  $M_* - M_h$  relation and the lack of an exponential cutoff in the GSMF. These indicate that the thermal stellar feedback is unable to quench star formation like is observed in massive galaxies.

Comparing SFR with stellar mass, the simulated galaxies lie along a tightly correlated “star forming main sequence.” The simulated galaxies match observations by Kajisawa et al. (2010) at  $z \geq 3$ , but there is a slight discrepancy at  $z = 2$  between simulations and observations. At a given stellar mass, the simulated SFRs and correspondingly, the sSFRs, are  $\sim 2$  times lower than the observed values at  $9.5 < \log(M_*/M_\odot) < 10.5$ . The high sSFRs in low mass haloes at  $z = 2$  suggests that there needs to be a significant amount of cold gas still present in these galaxies at  $z = 2$ . Although our model does a better job of delaying the star formation at early times than most SAMs and hydrodynamic simulations, after  $z = 3$  the simulated galaxies are forming too few stars.

Davé (2008) showed that the higher observed SFRs at  $z \leq 2$  can be explained by an evolving stellar IMF, which becomes increasingly bottom-light at high redshift. However, Marchesini et al. (2009) showed that when such a bottom light IMF was used to model observations, the resulting observed high-redshift GSMF contained less galaxies, making the discrepancy with model GSMFs worse.

Regarding the evolution of sSFRs at  $z > 3$ , our simulation results are consistent with the revised Stark et al. (2013) observations for a sample of galaxies with stellar masses centred around  $5 \times 10^9 M_\odot$ . The increasing sSFR at  $z \geq 4$  is consistent with increasing baryon accretion rates at larger redshift translating into larger sSFR in galaxies of fixed stellar mass. However, our simulated galaxies have lower sSFR values than observed at  $z = 2$ . Weinmann et al. (2012) argued that the correct sSFR evolution should follow naturally from the correct evolution of the GSMF. We see a slight deviation from the observed sSFR relation even though we match the GSMF. It must be noted that Weinmann et al. (2012) performed their analysis at  $z < 2$ , while our simulation has only reached at  $z = 2$ , where the observational estimates are less robust and might show some internal inconsistency among different galaxy properties (e.g. sSFR and GSMF).

There may also be another physical mechanism delaying star formation. Krumholz et al. (2011) and Krumholz & Dekel (2012) argue that star formation depends sensitively on a metallicity threshold. Until gas reaches this threshold, which coincidentally also delays the formation of H<sub>2</sub>, star formation is delayed in low mass galaxies at  $z > 3$ , which leaves sufficient cold gas at  $z = 2$  to increase the sSFR of these galaxies to the observed values.

To compare the model with observations of the local Universe, the inner  $16 h^{-1}$  Mpc of the fiducial run was simulated with gas to  $z = 0$ . The  $M_* - M_h$  relation is reproduced

at low masses ( $M_h = 10^{11} M_\odot$ ) and an over cooling problem still exists at high masses ( $M_h = 10^{12} M_\odot$ ). In the intermediate mass regime, we are below the relation by a factor of two. We also match the observed star forming main sequence quite well, although we are a bit above the relation throughout the entire mass range. These results indicate that our model does not fare so well at  $z = 0$  as at high redshifts but the errors are low when compared to many semi-analytic models and simulations (Guo et al. 2011; Davé 2008).

Two low resolution ( $2 \times 256^3$  particles) realisations of the fiducial volume were simulated to test the effect of resolution and importance of ESF. Both volumes used the same the same physics as the fiducial volume, but one had ESF turned off. The low resolution volume fiducial simulation compares well with the high resolution fiducial run and observations for galaxies with  $M_* > 10^{9.5} M_\odot$  (20 star particles). However, the re-simulation without ESF has too many galaxies with  $M_* > 10^{10} M_\odot$ .

Altogether, our results suggest that stellar feedback is one of the most important factors regulating star formation in  $M_{halo} < 10^{12} M_\odot$  galaxies. What is most important is *when* the feedback occurs rather than simply the amount of feedback energy. Simply increasing and decreasing the feedback energy will only set the normalisation i.e., the total stellar mass of present at  $z = 0$ , but the key is delaying star formation in low mass galaxies. When we include stellar feedback immediately after a star forms until supernovae stop exploding after 30 Myr, star formation is significantly delayed in low mass galaxies. In this way, we account for the downsizing in galaxy populations by delaying the star formation in low mass galaxies with our stellar feedback model and thus reconcile a couple key aspects of a  $\Lambda$ CDM cosmology with observations.

## ACKNOWLEDGEMENTS

We thank the anonymous referee for insightful comments which helped us in improving the paper. We are grateful to Ben Moster for providing his data in electronic format. We thank Arjen van der Wel and Aaron Dutton for valuable discussions. The simulations were performed on the THEO cluster of the Max-Planck-Institut für Astronomie at the Rechenzentrum in Garching; the clusters hosted on SHARCNET, part of ComputeCanada and the Milky Way supercomputer, funded by the Deutsche Forschungsgemeinschaft (DFG) through Collaborative Research Center (SFB 881) The Milky Way System (subproject Z2), hosted and co-funded by the Jülich Supercomputing Center (JSC). We greatly appreciate the contributions of these computing allocations. RK, AVM and GS also acknowledge support from SFB 881 “The Milky Way System” (subproject A1) of the German Research Foundation (DFG). CBB acknowledges Max-Planck-Institut für Astronomie for its hospitality and financial support through the Sonderforschungsbereich SFB 881 (subproject A1) of the DFG.

## REFERENCES

Agertz O., Kravtsov A. V., Leitner S. N., Gnedin N. Y., 2013, *ApJ*, 770, 25

Agertz O., Teyssier R., Moore B., 2011, *MNRAS*, 410, 1391  
 Alongi M., Bertelli G., Bressan A., Chiosi C., Fagotto F., Greggio L., Nasi E., 1993, *A&AS*, 97, 851  
 Behroozi P. S., Conroy C., Wechsler R. H., 2010, *ApJ*, 717, 379  
 Behroozi P. S., Wechsler R. H., Conroy C., 2013a, *ApJL*, 762, L31  
 Behroozi P. S., Wechsler R. H., Conroy C., 2013b, *ApJ*, 770, 57  
 Benson A. J., Bower R. G., Frenk C. S., Lacey C. G., Baugh C. M., Cole S., 2003, *ApJ*, 599, 38  
 Bouché N. et al., 2010, *ApJ*, 718, 1001  
 Bouwens R. et al., 2012, arXiv:1211.2230  
 Bouwens R. J. et al., 2011, *ApJ*, 737, 90  
 Bower R. G., Benson A. J., Crain R. A., 2012, *MNRAS*, 422, 2816  
 Bower R. G., Benson A. J., Malbon R., Helly J. C., Frenk C. S., Baugh C. M., Cole S., Lacey C. G., 2006, *MNRAS*, 370, 645  
 Bressan A., Fagotto F., Bertelli G., Chiosi C., 1993, *A&AS*, 100, 647  
 Brinchmann J., Charlot S., White S. D. M., Tremonti C., Kauffmann G., Heckman T., Brinkmann J., 2004, *MNRAS*, 351, 1151  
 Brook C. B. et al., 2011, *MNRAS*, 415, 1051  
 Brook C. B., Stinson G., Gibson B. K., Wadsley J., Quinn T., 2012, *MNRAS*, 424, 1275  
 Chabrier G., 2003, *PASP*, 115, 763  
 Conroy C., Wechsler R. H., 2009, *ApJ*, 696, 620  
 Conroy C., Wechsler R. H., Kravtsov A. V., 2006, *ApJ*, 647, 201  
 Crain R. A. et al., 2009, *MNRAS*, 399, 1773  
 Cucciati O. et al., 2012, *A&A*, 539, A31  
 Daddi E. et al., 2007, *ApJ*, 670, 156  
 Dalla Vecchia C., Schaye J., 2008, *MNRAS*, 387, 1431  
 Dalla Vecchia C., Schaye J., 2012, *MNRAS*, 426, 140  
 Damen M., Förster Schreiber N. M., Franx M., Labbé I., Toft S., van Dokkum P. G., Wuyts S., 2009, *ApJ*, 705, 617  
 Davé R., 2008, *MNRAS*, 385, 147  
 Davé R., Finlator K., Oppenheimer B. D., 2011a, *MNRAS*, 416, 1354  
 Davé R., Oppenheimer B. D., Finlator K., 2011b, *MNRAS*, 415, 11  
 De Lucia G., Springel V., White S. D. M., Croton D., Kauffmann G., 2006, *MNRAS*, 366, 499  
 Dunne L. et al., 2009, *MNRAS*, 394, 3  
 Dutton A. A., van den Bosch F. C., Dekel A., 2010, *MNRAS*, 405, 1690  
 Elbaz D. et al., 2007, *A&A*, 468, 33  
 Fanidakis N., Baugh C. M., Benson A. J., Bower R. G., Cole S., Done C., Frenk C. S., 2011, *MNRAS*, 410, 53  
 Fontanot F., De Lucia G., Monaco P., Somerville R. S., Santini P., 2009, *MNRAS*, 397, 1776  
 Gerritsen J., Icke V., 1997, in *Revista Mexicana de Astronomia y Astrofisica Conference Series*, Vol. 6, *Revista Mexicana de Astronomia y Astrofisica Conference Series*, Franco J., Terlevich R., Serrano A., eds., p. 261  
 González V., Labbé I., Bouwens R. J., Illingworth G., Franx M., Kriek M., Brammer G. B., 2010, *ApJ*, 713, 115  
 Governato F. et al., 2010, *Nature*, 463, 203  
 Guedes J., Callegari S., Madau P., Mayer L., 2011, *ApJ*, 742, 76

- Guo Q. et al., 2011, *MNRAS*, 413, 101
- Guo Q., White S., Li C., Boylan-Kolchin M., 2010, *MNRAS*, 404, 1111
- Hopkins A. M., 2004, *ApJ*, 615, 209
- Hopkins P. F., Quataert E., Murray N., 2011, *MNRAS*, 417, 950
- Kajisawa M., Ichikawa T., Yamada T., Uchimoto Y. K., Yoshikawa T., Akiyama M., Onodera M., 2010, *ApJ*, 723, 129
- Karim A. et al., 2011, *ApJ*, 730, 61
- Kauffmann G., White S. D. M., Guiderdoni B., 1993, *MNRAS*, 264, 201
- Kawata D., Gibson B. K., 2003, *MNRAS*, 340, 908
- Komatsu E. et al., 2011, *ApJS*, 192, 18
- Krumholz M. R., Dekel A., 2012, *ApJ*, 753, 16
- Krumholz M. R., Leroy A. K., McKee C. F., 2011, *ApJ*, 731, 25
- Larson D. et al., 2011, *ApJS*, 192, 16
- Lee K.-S. et al., 2012, *ApJ*, 752, 66
- Li C., White S. D. M., 2009, *MNRAS*, 398, 2177
- Lilly S. J., Le Fevre O., Hammer F., Crampton D., 1996, *ApJL*, 460, L1
- Lopez L. A., Krumholz M. R., Bolatto A. D., Prochaska J. X., Ramirez-Ruiz E., 2011, *ApJ*, 731, 91
- Ly C., Lee J. C., Dale D. A., Momcheva I., Salim S., Staudaher S., Moore C. A., Finn R., 2011, *ApJ*, 726, 109
- Macciò A. V., Dutton A. A., van den Bosch F. C., 2008, *MNRAS*, 391, 1940
- Macciò A. V., Dutton A. A., van den Bosch F. C., Moore B., Potter D., Stadel J., 2007, *MNRAS*, 378, 55
- Macciò A. V., Stinson G., Brook C. B., Wadsley J., Couchman H. M. P., Shen S., Gibson B. K., Quinn T., 2012, *ApJL*, 744, L9
- Madau P., Ferguson H. C., Dickinson M. E., Giavalisco M., Steidel C. C., Fruchter A., 1996, *MNRAS*, 283, 1388
- Marchesini D., van Dokkum P. G., Förster Schreiber N. M., Franx M., Labbé I., Wuyts S., 2009, *ApJ*, 701, 1765
- Martin C. L., 2005, *ApJ*, 621, 227
- McCarthy I. G., Schaye J., Font A. S., Theuns T., Frenk C. S., Crain R. A., Dalla Vecchia C., 2012, *MNRAS*, 427, 379
- Moster B. P., Naab T., White S. D. M., 2013, *MNRAS*, 428, 3121
- Moster B. P., Somerville R. S., Maulbetsch C., van den Bosch F. C., Macciò A. V., Naab T., Oser L., 2010, *ApJ*, 710, 903
- Munshi F. et al., 2013, *ApJ*, 766, 56
- Murray N., Ménard B., Thompson T. A., 2011, *ApJ*, 735, 66
- Murray N., Quataert E., Thompson T. A., 2010, *ApJ*, 709, 191
- Noeske K. G. et al., 2007, *ApJL*, 660, L43
- Oppenheimer B. D., Davé R., 2006, *MNRAS*, 373, 1265
- Oppenheimer B. D., Davé R., 2008, *MNRAS*, 387, 577
- Oppenheimer B. D., Davé R., Kereš D., Fardal M., Katz N., Kollmeier J. A., Weinberg D. H., 2010, *MNRAS*, 406, 2325
- Pannella M. et al., 2009, *ApJL*, 698, L116
- Peacock J. A., Smith R. E., 2000, *MNRAS*, 318, 1144
- Pellegrini E. W., Baldwin J. A., Ferland G. J., 2011, *ApJ*, 738, 34
- Peng Y.-j. et al., 2010, *ApJ*, 721, 193
- Press W. H., Schechter P., 1974, *ApJ*, 187, 425
- Puchwein E., Springel V., 2013, *MNRAS*, 428, 2966
- Reed D., Governato F., Quinn T., Gardner J., Stadel J., Lake G., 2005, *MNRAS*, 359, 1537
- Robotham A. S. G., Driver S. P., 2011, *MNRAS*, 413, 2570
- Rujopakarn W. et al., 2010, *ApJ*, 718, 1171
- Salim S. et al., 2007, *ApJS*, 173, 267
- Santini P. et al., 2012, *A&A*, 538, A33
- Sawala T., Guo Q., Scannapieco C., Jenkins A., White S., 2011, *MNRAS*, 413, 659
- Schaye J., Dalla Vecchia C., 2008, *MNRAS*, 383, 1210
- Shen S., Wadsley J., Stinson G., 2010, *MNRAS*, 407, 1581
- Sheth R. K., Mo H. J., Tormen G., 2001, *MNRAS*, 323, 1
- Sheth R. K., Tormen G., 2004, *MNRAS*, 350, 1385
- Smolčić V. et al., 2009, *ApJ*, 690, 610
- Somerville R. S., Primack J. R., 1999, *MNRAS*, 310, 1087
- Springel V., Di Matteo T., Hernquist L., 2005, *MNRAS*, 361, 776
- Springel V., Hernquist L., 2003, *MNRAS*, 339, 289
- Stark D. P., Ellis R. S., Bunker A., Bundy K., Targett T., Benson A., Lacy M., 2009, *ApJ*, 697, 1493
- Stark D. P., Schenker M. A., Ellis R., Robertson B., McLure R., Dunlop J., 2013, *ApJ*, 763, 129
- Stinson G., Seth A., Katz N., Wadsley J., Governato F., Quinn T., 2006, *MNRAS*, 373, 1074
- Stinson G. S., Brook C., Macciò A. V., Wadsley J., Quinn T. R., Couchman H. M. P., 2013, *MNRAS*, 428, 129
- Thacker R. J., Couchman H. M. P., 2000, *ApJ*, 545, 728
- van den Bosch F. C. et al., 2007, *MNRAS*, 376, 841
- van der Burg R. F. J., Hildebrandt H., Erben T., 2010, *A&A*, 523, A74
- Wadsley J. W., Stadel J., Quinn T., 2004, *New Astronomy*, 9, 137
- Weiner B. J. et al., 2009, *ApJ*, 692, 187
- Weinmann S. M., Neistein E., Dekel A., 2011, *MNRAS*, 417, 2737
- Weinmann S. M., Pasquali A., Oppenheimer B. D., Finlator K., Mendel J. T., Crain R. A., Macciò A. V., 2012, *MNRAS*, 426, 2797
- Whitaker K. E. et al., 2011, *ApJ*, 735, 86
- Whitaker K. E., van Dokkum P. G., Brammer G., Franx M., 2012, *ApJL*, 754, L29
- White S. D. M., Frenk C. S., 1991, *ApJ*, 379, 52
- White S. D. M., Rees M. J., 1978, *MNRAS*, 183, 341
- Wilkins S. M., Trentham N., Hopkins A. M., 2008, *MNRAS*, 385, 687
- Wuyts S. et al., 2011, *ApJ*, 738, 106
- Yang X., Mo H. J., van den Bosch F. C., 2003, *MNRAS*, 339, 1057
- Zheng X. Z., Dole H., Bell E. F., Le Floch E., Rieke G. H., Rix H.-W., Schiminovich D., 2007, *ApJ*, 670, 301